Applied and
Computational
Mechanics

Analytic solution of simplified Cardan's shaft model

M. Zajíček[a,*], J. Dupal[a]

[a]*Faculty of Applied Sciences, University of West Bohemia, Univerzitní 22, 306 14 Plzeň, Czech Republic*

Abstract

Torsional oscillations and stability assessment of the homokinetic Cardan shaft with a small misalignment angle is described in this paper. The simplified mathematical model of this system leads to the linearized equation of the Mathieu's type. This equation with and without a stationary damping parameter is considered. The solution of the original differential equation is identical with those one of the Fredholm's integral equation with degenerated kernel assembled by means of a periodic Green's function. The conditions of solvability of such problem enable the identification of the borders between stability and instability regions. These results are presented in the form of stability charts and they are verified using the Floquet theory. The correctness of oscillation results for the system with periodic stiffness is then validated by means of the Runge-Kutta integration method.
© 2014 University of West Bohemia. All rights reserved.

Keywords: Cardan shaft, analytic periodic solution, stability assessment, linearized equation, Mathieu's equation

1. Introduction

The Cardan's shaft is used as a component of many mechanisms for the transmission of torque through angularly misaligned rotating shafts. Typical applications can be found, e.g., in automobile industry or shipbuilding. It could be said that the problems relating to angularly misaligned shafts are so far at the subject of research. This can be illustrated by the development of various types of joints for transfer constant velocity, see, e.g., [16]. The typical design of the Cardan's shaft is composed of two Hooke's joints in series and mutually connected with a shaft that usually enables an axial dilatation. A major problem with the use of Hooke's joint, also known as the Cardan's joint or the universal joint, is that it transforms a constant input speed to a periodically fluctuating one. This means that the dynamic system with these joints is parametrically excited. It introduces a number of specific resonance conditions or dynamic instability of the system. The main goal of analyzing such systems is assessment of the instability conditions as well as the periodic solution of the steady state motion.

It seems Porter [13] to be the first who predicted the critical speed ranges associated with such a system. A linearized one-degree-of-freedom (1 DOF) model was considered to predict the two primary parametric resonance zones of a stability chart obtained using the Floquet theory [9]. Investigation was concerned, among others, with the effects of parameters such as stiffness ratio and joint angle on the critical speed ranges. These analyses were later extended to a nonlinear model given in [14]. The first approximation of the Krylov-Bogoliubov method was used to get the system behavior in the two primary parametric resonance zones. Porter and Gregory [14] showed that the system ultimately executes a limit cycle of oscillation and that (in certain critical speed ranges) the amplitude of this oscillation is large if the system is lightly

*Corresponding author. Tel.: +420 377 632 328, e-mail: zajicek@kme.zcu.cz.

damped. The stability problem was studied through Poincaré-Lyapunov method described, e.g., in [10]. Zahradka [17] brought the solution for a 1 DOF driving system incorporating the Cardan shafts by means of the approximate Van der Pol's method of slowly-varying coefficients. The resulting nonlinear equation of motion with periodic coefficients was investigated in the region of subharmonic and subultraharmonic resonance. Zahradka showed that a number of solutions exist for one tuning coefficient of a system and the width of attraction domains depends mainly on the system damping and the angular misalignment of the Hooke's joints. Chang [5] revisited nonlinear equation presented in [13] and obtained the higher order stability map for the damped system by using a perturbation technique. Moreover, the application of higher order averaging (see [12]) to the equation of motion leads to amplitude equations consisting of a finite number of terms including quadratic and cubic nonlinearities.

Porter [15] investigated the problem in [14] by considering a 2 DOF model and established the instability conditions as well as the amplitudes of the steady state motion. Asokanthan and Hwang [1] also solved the system with a 2 DOF. They used the method of averaging and established the closed form instability conditions associated with combined resonance. The same problem of instabilities was investigated through calculations of the Lyapunov exponent in [3]. In both cases mentioned above, only linearized models were employed, and as a result the critical speed ranges due to quasi-periodic and chaotic motion were not predicted. Later, Asokanthan and Methan [2] considered a nonlinear model and showed via numerical simulations that the system may exhibit chaotic behavior under certain circumstances. The dynamic stability problem was solved in [4] by means of a monodromy matrix method. Linearized n DOF system was solved by Zeman in [18, 19] and Kotera in [11].

The goal of the present study is to apply to the Cardan's shaft problem solving methodology developed by the authors in [8]. The use of this solution is suitable for a linear system with periodically varying stiffness and excitation, see [7]. Therefore, the governing linearized equation representing the torsional motion of the system is derived. The model with and without a stationary damping parameter is considered. The periodic analytic solutions in a steady state including the boundary curves of (in)stability regions are determined using the presented method.

2. Governing equation

For the purposes of the present study, the simplified model of the homokinetic Cardan's shaft which is depicted in Fig. 1 is derived. Let us assume that the torsional stiffness of shafts 1 and 3 is closing to infinity, and so $\varphi_2 \equiv \varphi_1$ and $\varphi_5 \equiv \varphi_6$. Furthermore, the rotary inertia of disks 1 and 6 is dominant and the others are neglected. The transformation relations between φ_3, φ_2 and φ_4, φ_5 have the form (see, e.g. [6])

$$\tan \varphi_3 = \tan \varphi_2 \cos \delta = \tan \varphi_1 \cos \delta \qquad \text{and} \qquad \tan \varphi_4 = \tan \varphi_5 \cos \delta = \tan \varphi_6 \cos \delta \,, \quad (1)$$

where the initial configuration of the Hooke's joints is shown in position on Fig. 1. However, if the initial position of joints is turned at $90°$, the relations have the form

$$\tan \varphi_3 = \frac{\tan \varphi_2}{\cos \delta} = \frac{\tan \varphi_1}{\cos \delta} \qquad \text{and} \qquad \tan \varphi_4 = \frac{\tan \varphi_5}{\cos \delta} = \frac{\tan \varphi_6}{\cos \delta} \,. \quad (2)$$

Parameter δ denotes an angular misalignment. Let us assume that the angle δ is small. For this reason, the approximations are used as follows:

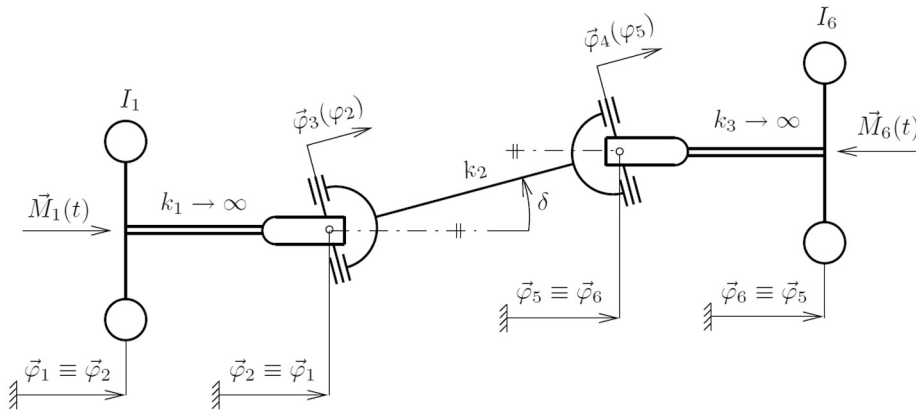$$\cos \delta \approx 1 - \delta^2/2 \,, \qquad 1/\cos \delta \approx 1 + \delta^2/2 \,. \quad (3)$$

Fig. 1. Simplified scheme of Cardan shaft

Then equations (1) and (2) can be rewritten by means of (3) as

$$\tan \varphi_3 \approx (1 \mp \frac{\delta^2}{2}) \tan \varphi_1 \qquad \text{and} \qquad \tan \varphi_4 \approx (1 \mp \frac{\delta^2}{2}) \tan \varphi_6 \qquad (4)$$

with respect to both initial configurations of the Hooke's joints. When the functions $\tan \varphi_3$ and $\tan \varphi_4$ are expanded to the Taylor series with regard to the first two terms,

$$\tan \varphi_3 = \tan(\varphi_1 + \Delta\varphi_1) \approx \tan \varphi_1 + \frac{1}{\cos^2 \varphi_1} \Delta\varphi_1 \,,$$

$$\tan \varphi_4 = \tan(\varphi_6 + \Delta\varphi_6) \approx \tan \varphi_6 + \frac{1}{\cos^2 \varphi_6} \Delta\varphi_6 \,, \qquad (5)$$

it is simply proved with the aid of (4) that the increments $\Delta\varphi_1$ and $\Delta\varphi_6$ are as follows:

$$\Delta\varphi_1 \approx \mp\frac{\delta^2}{2} \tan \varphi_1 \cos^2 \varphi_1 = \mp\frac{\delta^2}{4} \sin 2\varphi_1 \,,$$

$$\Delta\varphi_6 \approx \mp\frac{\delta^2}{2} \tan \varphi_6 \cos^2 \varphi_6 = \mp\frac{\delta^2}{4} \sin 2\varphi_6 \,. \qquad (6)$$

Therefore, the angles φ_3 and φ_4 are approximated such as

$$\varphi_3 = \varphi_1 + \Delta\varphi_1 \approx \varphi_1 \mp \frac{\delta^2}{4} \sin 2\varphi_1 \qquad \text{and} \qquad \varphi_4 = \varphi_6 + \Delta\varphi_6 \approx \varphi_6 \mp \frac{\delta^2}{4} \sin 2\varphi_6 \,. \qquad (7)$$

The equations of motion in terms of the twist variables $\boldsymbol{\varphi} = [\varphi_1, \varphi_6]^{\mathrm{T}}$ may be derived using Lagrange's equations

$$\frac{\mathrm{d}}{\mathrm{d}t} \left(\frac{\partial E_{\mathrm{k}}}{\partial \dot{\boldsymbol{\varphi}}} \right) - \frac{\partial E_{\mathrm{k}}}{\partial \boldsymbol{\varphi}} = \frac{\delta W}{\delta \boldsymbol{\varphi}} - \frac{\partial E_{\mathrm{p}}}{\partial \boldsymbol{\varphi}} \,, \qquad (8)$$

where

$$E_{\mathrm{k}} = \frac{1}{2} I_1 \dot{\varphi}_1{}^2 + \frac{1}{2} I_6 \dot{\varphi}_6{}^2 \qquad \text{and} \qquad E_{\mathrm{p}} = \frac{1}{2} k_2 \left[\varphi_4(\varphi_6) - \varphi_3(\varphi_1) \right]^2 \qquad (9)$$

is kinetic and potential energy of the system, respectively. The virtual work δW of non-conservative forces takes the form

$$\delta W = M_1(t) \delta\varphi_1 - M_6(t) \delta\varphi_6 \,. \qquad (10)$$

217

After substitution (9) and (10) into (8), and after some term rearrangements, the two equations of motion can be expressed in the form

$$I_1 \ddot{\varphi}_1 + k_2(\varphi_1 - \varphi_6) \mp k_2(\varphi_1 - \varphi_6) \frac{\delta^2}{2} \cos 2\varphi_1 = M_1(t) \,,$$

$$I_6 \ddot{\varphi}_6 - k_2(\varphi_1 - \varphi_6) \pm k_2(\varphi_1 - \varphi_6) \frac{\delta^2}{2} \cos 2\varphi_6 = -M_6(t) \,. \tag{11}$$

The system of equations (11) is further linearized using the following simplifications:

$$\cos 2\varphi_1 = \cos 2(\omega t + \Delta\varphi_1) \doteq \cos 2\omega t \,, \quad \cos 2\varphi_6 = \cos 2(\omega t + \Delta\varphi_6) \doteq \cos 2\omega t \,. \tag{12}$$

Multiplying the first equation in (11) by $1/I_1$ and the second one (11) by $1/I_6$, and subtracting the two resulting equations lead to

$$\ddot{\varphi} + \Omega^2 (1 \mp \varepsilon \cos 2\omega t)\varphi = \frac{M_1(t)}{I_1} + \frac{M_6(t)}{I_6} \,, \tag{13}$$

which is the equation of the relative torsional vibrations of the Cardan's shaft shown in Fig. 1. In the above equation,

$$\varepsilon = \frac{\delta^2}{2} \,, \qquad \Omega^2 = \frac{k_2}{I_1} + \frac{k_2}{I_6} \qquad \text{and} \qquad \varphi = \varphi_1 - \varphi_6 \,, \tag{14}$$

where ε is a measure of stiffness modulation. The signs $\mp$ in (13) indicate what the initial configuration of the Hooke's joints is considered. After dimensionless transformation

$$\tau = \Omega t \qquad \text{and} \qquad \eta = \omega/\Omega \tag{15}$$

and some arrangements

$$\ddot{\varphi}(t) = \Omega^2 \varphi''(\tau) \qquad \text{and} \qquad \omega t = \eta\tau \,, \tag{16}$$

the equation of motion (13) is further written as

$$\varphi'' + (1 \mp \varepsilon \cos 2\eta\tau)\varphi = \frac{1}{\Omega^2} \left(\frac{M_1(\tau)}{I_1} + \frac{M_6(\tau)}{I_6} \right) \,. \tag{17}$$

Let us consider that the system is damped. When only a stationary damping is taken into account, the equations of motion (13) and (17) can be extended and rewritten in the form

$$\ddot{\varphi} + 2D\Omega\dot{\varphi} + \Omega^2 (1 \mp \varepsilon \cos 2\omega t)\varphi = \frac{M_1(t)}{I_1} + \frac{M_6(t)}{I_6} \,, \tag{18}$$

$$\varphi'' + 2D\varphi' + (1 \mp \varepsilon \cos 2\eta\tau)\varphi = \frac{1}{\Omega^2} \left(\frac{M_1(\tau)}{I_1} + \frac{M_6(\tau)}{I_6} \right) \,, \tag{19}$$

respectively, where D is a damping ratio. If the functions $M_1(t)$ and $M_6(t)$ are periodic with period $T = 2\pi/\omega$, the steady state solution of the derived equation of motion with and/or without damping can be found analytically.

3. Analytic solution in steady state and stability assessment

The presented method of solution is based on the knowledge of a periodic Green's function $H(t)$ which is constructed as a response of the stationary part of the equation of motion to the T-periodic Dirac chain, see [8]. While respecting (18) where the effect of damping is considered, equation for finding $H(t)$ can be written as

$$\ddot{H}(t) + 2D\Omega\dot{H}(t) + \Omega^2 H(t) = \frac{1}{T} \sum_{n=-\infty}^{\infty} e_n(t), \qquad (20)$$

where

$$e_n(t) = \mathrm{e}^{\mathrm{i}n\omega t} \qquad \text{and} \qquad \mathrm{i}^2 = -1. \qquad (21)$$

Superposition principle in solving (20) leads to finding the periodic Green's function in the form

$$H(t) = \frac{1}{T} \sum_{n=-\infty}^{\infty} L_n e_n(t), \qquad (22)$$

where

$$L_n = \frac{1}{\Omega^2} \frac{1}{1 + 2\mathrm{i}Dn\eta - n^2\eta^2}. \qquad (23)$$

Including the parametric term $(\Omega^2 \varepsilon \cos 2\omega t)\varphi$ into the exitation, the steady state response corresponding to equation (18) may then be expressed as a sum of convolution integrals

$$\varphi(t) = \pm\varepsilon \int_0^T H(t-s)k(s)\varphi(s)\,\mathrm{d}s + \int_0^T H(t-s)f(s)\,\mathrm{d}s, \qquad (24)$$

where

$$k(s) = \Omega^2 \cos 2\omega s \qquad \text{and} \qquad f(s) = \frac{M_1(s)}{I_1} + \frac{M_6(s)}{I_6}. \qquad (25)$$

With regard to the solution mentioned in [8], the function $\varphi(t)$ can then be written in the form

$$\varphi(t) = \mathbf{e}^{\mathrm{T}}(t)\left[\mathbf{I} \pm \varepsilon\left(\mathbf{I} \mp \varepsilon\mathbf{L}\mathbf{H}\right)^{-1}\mathbf{L}\mathbf{H}\right]\mathbf{L}\mathbf{f}, \qquad (26)$$

where $\mathbf{I}$ is the infinity identity matrix, $\mathbf{L}$ is the infinity diagonal matrix

$$\mathbf{L} = \mathrm{diag}\{L_n\} \qquad (27)$$

and $\mathbf{H}$ is a symmetric matrix defined as

$$\mathbf{H} = \frac{1}{2}\Omega^2 \begin{bmatrix} \ddots & \vdots & \vdots & \vdots & \vdots & \vdots & \iddots \\ \cdots & 0 & 0 & 1 & 0 & 0 & \cdots \\ \cdots & 0 & 0 & 0 & 1 & 0 & \cdots \\ \cdots & 1 & 0 & 0 & 0 & 1 & \cdots \\ \cdots & 0 & 1 & 0 & 0 & 0 & \cdots \\ \cdots & 0 & 0 & 1 & 0 & 0 & \cdots \\ \iddots & \vdots & \vdots & \vdots & \vdots & \vdots & \ddots \end{bmatrix}. \qquad (28)$$

Further, the vectors in equation (26) are given as

$$\mathbf{e}(t) = [\ldots, e_{-n}(t), \ldots, e_{-1}(t), 1, e_1(t), \ldots, e_n(t), \ldots]^{\mathrm{T}}, \qquad (29)$$

$$\mathbf{f} = [\ldots, f_{-n}, \ldots, f_{-1}, f_0, f_1, \ldots, f_n, \ldots]^{\mathrm{T}} \qquad \text{with} \qquad f(t) = \mathbf{f}^{\mathrm{T}}\mathbf{e}(t). \qquad (30)$$

It is obvious that solving $\varphi(t)$ exists only if the matrix $\mathbf{I} \mp \varepsilon\mathbf{LH}$ is invertible. Then, the real (for a real system) eigenvalues $1/\varepsilon$ of the matrix $\mathbf{LH}$ determine the borders of (in)stability. However, the boundaries between the stable and unstable regions at combinations of parameters η and ε may occur not only for the ratio $\varphi(t+T)/\varphi(t) = 1$ but also for the ratio -1. While in the first case, the solution $\varphi(t)$ has a period T, in the second case it has a period $2T$. Hence, it follows that it is necessary to take into account the resonant stage with frequency $\omega/2$. The eigenvalues are then determined for a matrix $\mathbf{L}^*\mathbf{H}^*$, where

$$\mathbf{L}^* = \mathrm{diag}\left\{\ldots, L_{-n}, L_{-n+\frac{1}{2}}, L_{-n+1}, \ldots, L_0, \ldots, L_{n-1}, L_{n-\frac{1}{2}}, L_n, \ldots\right\} \tag{31}$$

and

$$\mathbf{H}^* = \frac{1}{2}\Omega^2 \begin{bmatrix} \ddots & \vdots & \vdots & \vdots & \vdots & \vdots & \vdots & \cdot^{\cdot^{\cdot}} \\ \cdots & 0 & 0 & 0 & 0 & 1 & 0 & \cdots \\ \cdots & 0 & 0 & 0 & 0 & 0 & 1 & \cdots \\ \cdots & 0 & 0 & 0 & 0 & 0 & 0 & \cdots \\ \cdots & 0 & 0 & 0 & 0 & 0 & 0 & \cdots \\ \cdots & 1 & 0 & 0 & 0 & 0 & 0 & \cdots \\ \cdots & 0 & 1 & 0 & 0 & 0 & 0 & \cdots \\ \cdot^{\cdot^{\cdot}} & \vdots & \vdots & \vdots & \vdots & \vdots & \vdots & \ddots \end{bmatrix}. \tag{32}$$

It has been proved in [8] that the spectra of matrices $\mathbf{LH}$ and $\mathbf{L}^*\mathbf{H}^*$ satisfy the condition

$$\mathbf{\Sigma}\left(\mathbf{LH}\right) \subset \mathbf{\Sigma}\left(\mathbf{L}^*\mathbf{H}^*\right). \tag{33}$$

The real calculations of $\varphi(t)$ or ε are not possible for an infinite system. Therefore, the finite systems of equations have to be solved. Let us denote the solutions $\varphi_N(t)$ and ε_N approximated by the system of $2N+1$ and $4N+1$ equations, respectively. The solutions are assumed to be correct, i.e. $\varphi_N(t) = \varphi(t)$ and $\varepsilon_N = \varepsilon$, if the conditions

$$\|\varphi_{N+1}(t) - \varphi_N(t)\| < \varepsilon_\varphi \ \ \text{for} \ \ \varphi_{N+1}, \varphi_N \in L_2(0,T) \qquad \text{and} \qquad \left(\frac{\varepsilon_{N+1}}{\varepsilon_N} - 1\right)^2 < \varepsilon_\lambda \tag{34}$$

are satisfied while the parameters ε_φ and ε_λ are small positive numbers.

4. Numerical results and discussion

As further shown in this section, the existence of the searched solution $\varphi(t)$ is closely related to the investigation of stability regions. The equation of motion derived for the Cardan's shaft has limitations in use only for small values of the parameter δ, and therefore it makes sense to analyze a limited zones of stability with respect to this parameter. As known, the problem of stability is not dependent on the excitation. Identified regions of stability have so general validity for the analyzed equation of motion that is of Mathieu's type. The following numerical computation of stability problems are performed for the number $N = 18$.

The stability chart of an undamped system is shown in Fig. 2. It is evident that the (in)stability borders are symmetric about the axis $\varepsilon = 0$ and that the system may become unstable for values $|\delta| < 30°$ only in small regions. It is also interesting that the stable regions are repeatedly divided by the (in)stability borders. This fact is well seen in Fig. 3 showing the values of the determinant $d = \det\left(\mathbf{I} - \varepsilon\mathbf{L}^*\mathbf{H}^*\right)$. This one takes only the non-negative values in the places
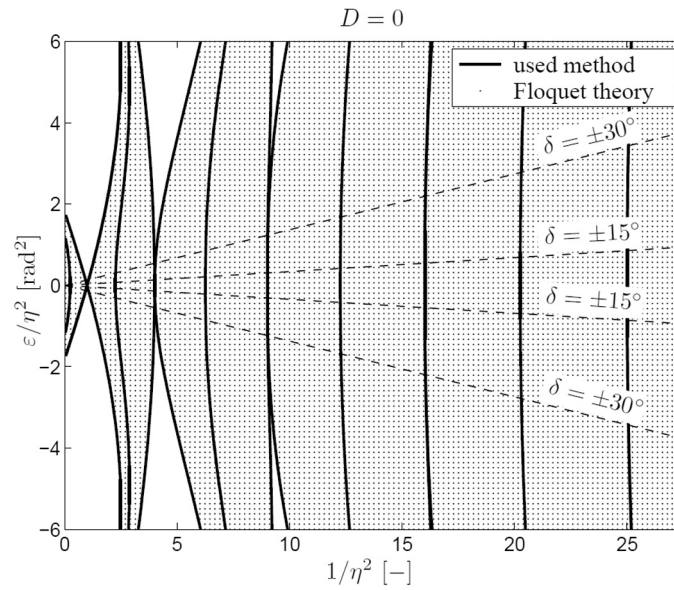
Fig. 2. Stable and unstable regions, problem without damping

of interest. Numerical experiments have demonstrated that there are double eigenvalues (points where $d = 0$). Fig. 3 also shows one important observation that is proved to be valid in all solved cases. The investigated systems with and without damping are stable when the determinant takes positive values.
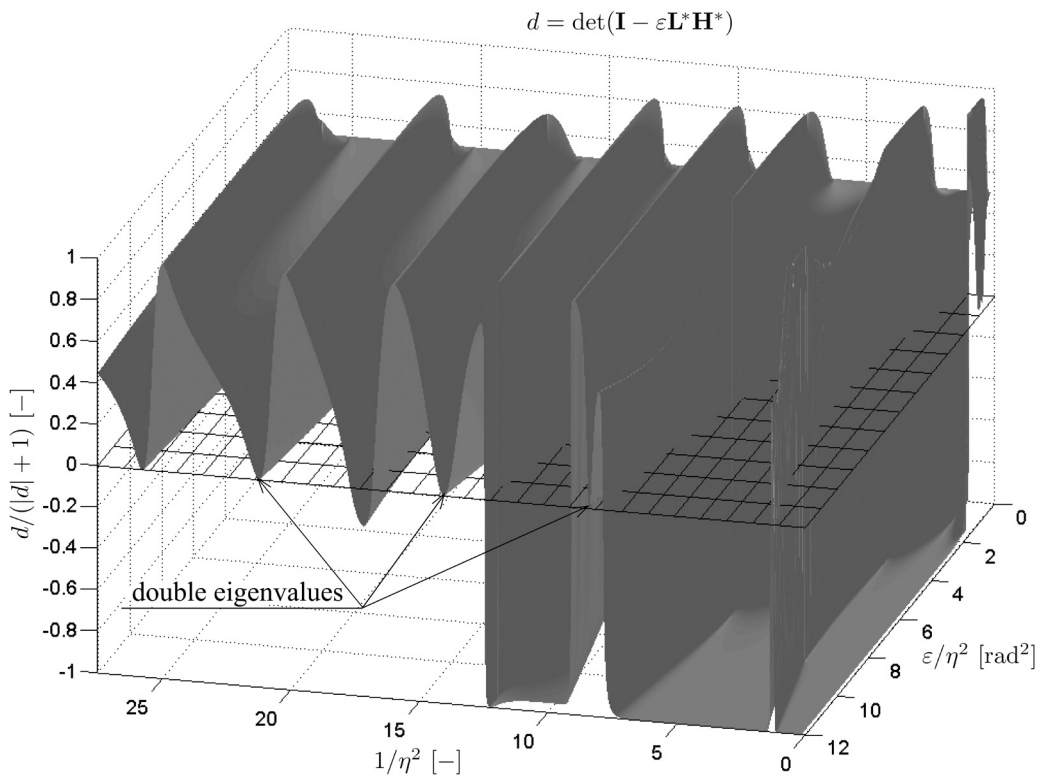

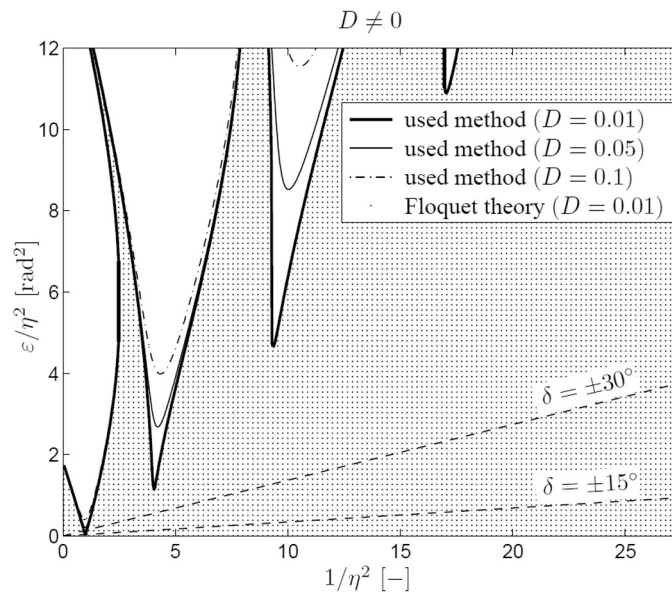Fig. 3. Calculated values of determinant d in stable and unstable regions, problem without damping

Fig. 4. Stable and unstable regions, problem with damping

The shape of the stable and unstable regions for different values of a damping ratio D is depicted in Fig. 4. The (in)stability borders are also symmetric about the axis $\varepsilon = 0$ as in the case $D = 0$, and therefore only the upper half ($\varepsilon \geq 0$) of the figure is presented. It is obvious from Fig. 4 that the system is stable for all values of η if $|\delta| < 15°$ and $D \geq 0.01$. In contrast, if the angle $\delta = \pm 30°$ and $D = 0.01$, the system is unstable for values close to $\eta = 1$. Furthermore, it is found that the unstable region of a set of zero measure do not occur in cases with damping. The correctness of detected boundaries is verified using Floquet theory [9]. It is clear from Figs. 2 and 4 that a very good agreement is found. The dot marks in both figures represent the points of stability.

The response calculation in steady state is performed for (17) and (19). It is supposed that the driving torque is

$$M_1(t) = M_1 = \text{constant}, \tag{35}$$

which is the typical characteristic of DC motors. The powered torque is then considered in the form of a Fourier series

$$M_6(t) = m_0 + \sum_{j=1}^{\infty} m_j \cos(j\omega t + \phi_j) \approx M_1 \left[r_0 + r_1 \cos(\omega t + \phi) + r_2 \cos 2\omega t \right], \tag{36}$$

while the moment is approximated by only the first three terms. Let us define the following ratios:

$$r_j = \frac{m_j}{M_1} \qquad \text{for} \qquad j = 0, 1, 2. \tag{37}$$

The right-hand side of equations (17) and (19) then takes the form

$$\frac{1}{\Omega^2} \left(\frac{M_1(\tau)}{I_1} + \frac{M_6(\tau)}{I_6} \right) = \frac{M_1}{k_2} \frac{I_1 I_6}{I_1 + I_6} \left\{ \frac{1}{I_1} + \frac{1}{I_6} \left[r_0 + r_1 \cos(\eta\tau + \phi) + r_2 \cos 2\eta\tau \right] \right\} =$$

$$= \frac{\varphi_{\mathrm{m}}}{1 + \lambda_{\mathrm{I}}} \left[\lambda_{\mathrm{I}} + r_0 + r_1 \cos(\eta\tau + \phi) + r_2 \cos 2\eta\tau \right], \tag{38}$$

where

$$\varphi_{\mathrm{m}} = \frac{M_1}{k_2} \qquad \text{and} \qquad \lambda_{\mathrm{I}} = \frac{I_6}{I_1}. \tag{39}$$

$$D = 0\,,\ \delta = 15°,\ 1/\eta^2 = 1\,,\ \varphi(0) = 0\,,\ \dot{\varphi}(0) = 0$$

(a)

$$D = 0.01\,,\ \delta = 30°,\ 1/\eta^2 = 1\,,\ \varphi(0) = 0\,,\ \dot{\varphi}(0) = 0$$
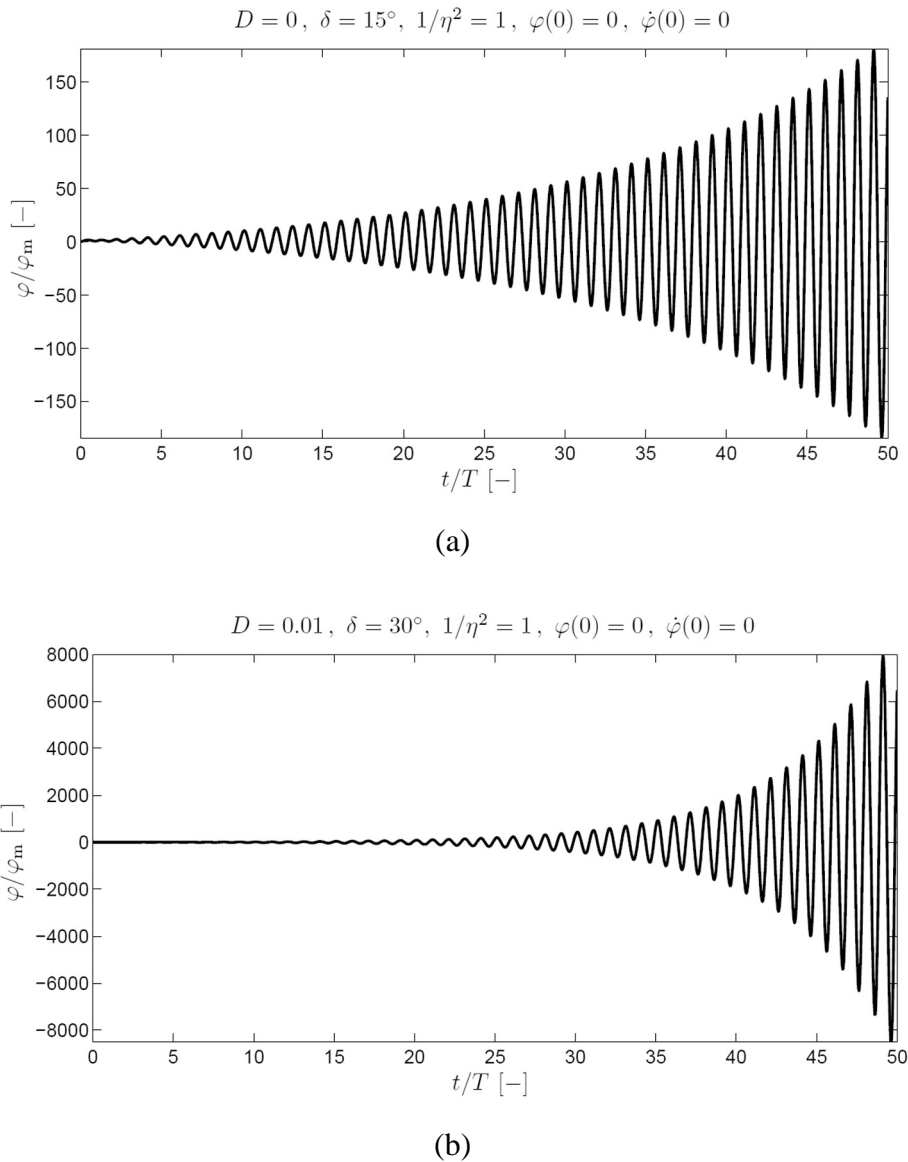

(b)

Fig. 5. Examples of calculation of response by the R-KI method in an unstable region

The above mentioned parameters are chosen for the numerical simulations as follows: $r_0 = 1.0$, $r_1 = 0.5$, $r_2 = 0.25$, $\phi = \pi/4$ and $\lambda_{\mathrm{I}} = 1$. The work also includes analyses of results for two values of an angular misalignment $\delta = \{15°, 30°\}$. The parameter N specifies the number of Fourier series terms used for the description of the function $\varphi(\tau)$ and is set with respect to the numerical experiments. The value $N = 14$ is used for all subsequent calculations.

Typical characteristics of the system without and with damping in the unstable region is shown in Fig. 5(a) and (b), respectively. The system without damping is unstable respecting both $\delta = 15°$ and $\delta = 30°$ while the system with damping is unstable only for $\delta = 30°$. It can be seen in Figs. 2 and 4. Because the analytic solution given in equation (26) is valid only in the stable regions, it is necessary to find solutions through other methods. The Runge-Kutta integration (R-KI) method implemented in MATLAB function `ode45` is used. It is clear that the system is unstable with respect to an increasing amplitude in both cases, see Fig. 5. Computations were done for equations (17) and (19) having on the left side the periodic term "$-\varepsilon\varphi\cos 2\eta\tau$".
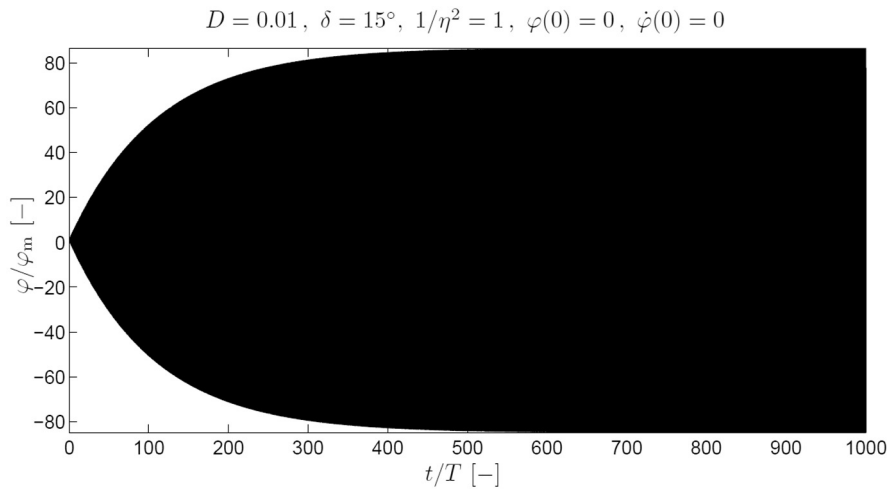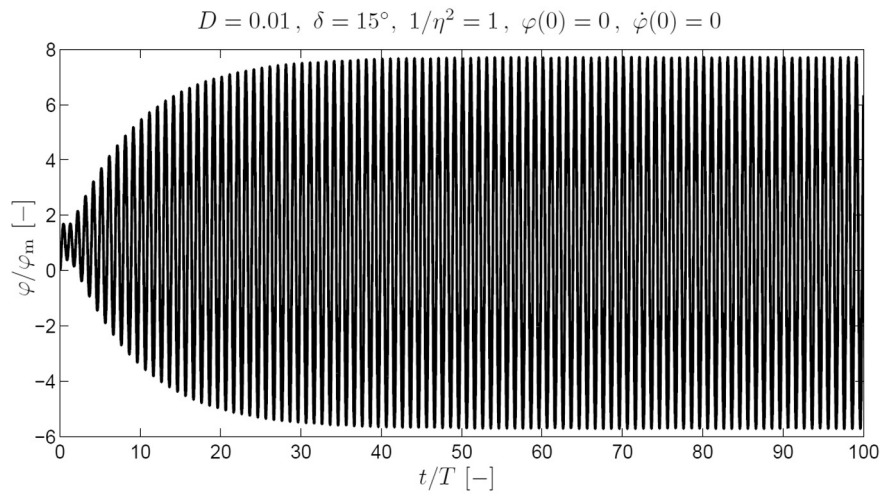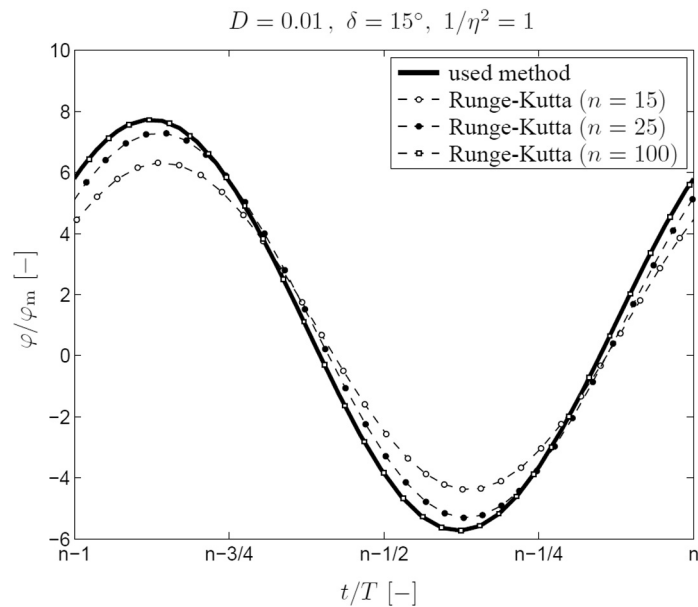
(a)
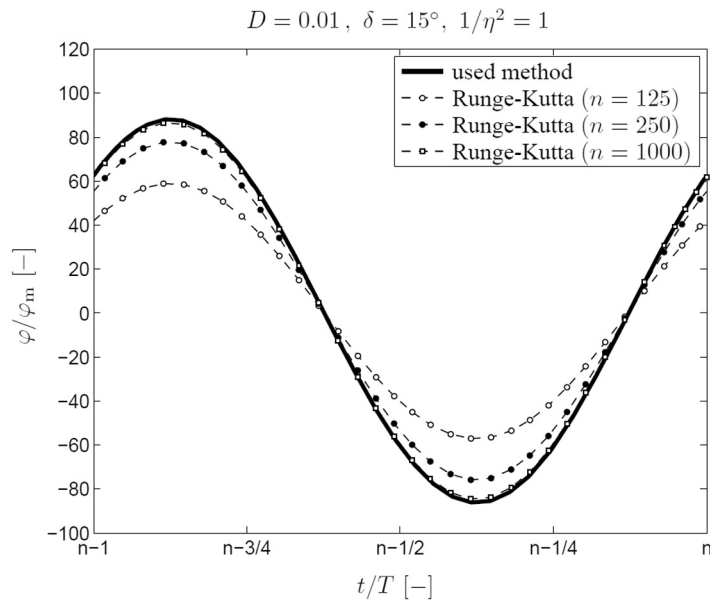
(b)

Fig. 6. Response in a stable region calculated by the R-KI method (a)–(b), and by the used method (b); considered periodic term "$-\varepsilon\varphi\cos 2\eta\tau$"

Response φ obtained for the similar parameters ($D = 0.01$, $\delta = 15°$, $\eta = 1$) but in the stable region is shown in Figs. 6 and 7. In the first case (Fig. 6), the equation of motion (19) with the periodic term "$-\varepsilon\varphi\cos 2\eta\tau$" is considered. Subsequently, the curves depicted in Fig. 7 correspond to the case where the periodic term is "$+\varepsilon\varphi\cos 2\eta\tau$". While the sign of this term has no influence on the stability charts because the (in)stability borders are symmetric about axis $\varepsilon = 0$, the effect on the response φ is apparent and it is caused by a different phase delay of excitation and stiffness modulation. Although the curves have similar shape, the ratio $\varphi/\varphi_\mathrm{m}$ gives significantly different values, see Figs. 6(b) and 7(b). It is also obvious in Figs. 6(a) and 7(a) that it is necessary to consider a different number of cycles t/T using R-KI method when comparable results with the analytic solution be provided.

$D = 0.01$, $\delta = 15°$, $1/\eta^2 = 1$, $\varphi(0) = 0$, $\dot{\varphi}(0) = 0$

(a)

$D = 0.01$, $\delta = 15°$, $1/\eta^2 = 1$

(b)

Fig. 7. Response in a stable region calculated by the R-KI method (a)–(b), and by the used method (b); considered periodic term "$+\varepsilon\varphi\cos 2\eta\tau$"

Previous examples of calculations made using the R-KI method show only the problems with homogeneous initial conditions. As known from the Floquet theory, the eigenvalues ρ of a monodromy matrix called the characteristic multipliers decide about the system stability. If all $\rho_i \in \mathbb{C}$, $\forall i$, satisfy the condition $|\rho_i| < 1$, then the system is stable and the solution φ corresponds to the stable limit cycle. This fact is demonstrated in Fig. 8. The same results using the R-KI method are obtained for the system with homogeneous and inhomogeneous ($\varphi(0) = -1$, $\dot{\varphi}(0) = 1$) initial conditions after a number of cycles $t/T = 25$. A very good agreement of the analytic and numeric results is shown in Fig. 8(c) and (d).

$D = 0.01$, $\delta = 15°$, $1/\eta^2 = 20$, $\varphi(0) = 0$, $\dot{\varphi}(0) = 0$

(a)

$D = 0.01$, $\delta = 15°$, $1/\eta^2 = 20$, $\varphi(0) = -1$, $\dot{\varphi}(0) = 1$

(b)

$D = 0.01$, $\delta = 15°$, $1/\eta^2 = 20$
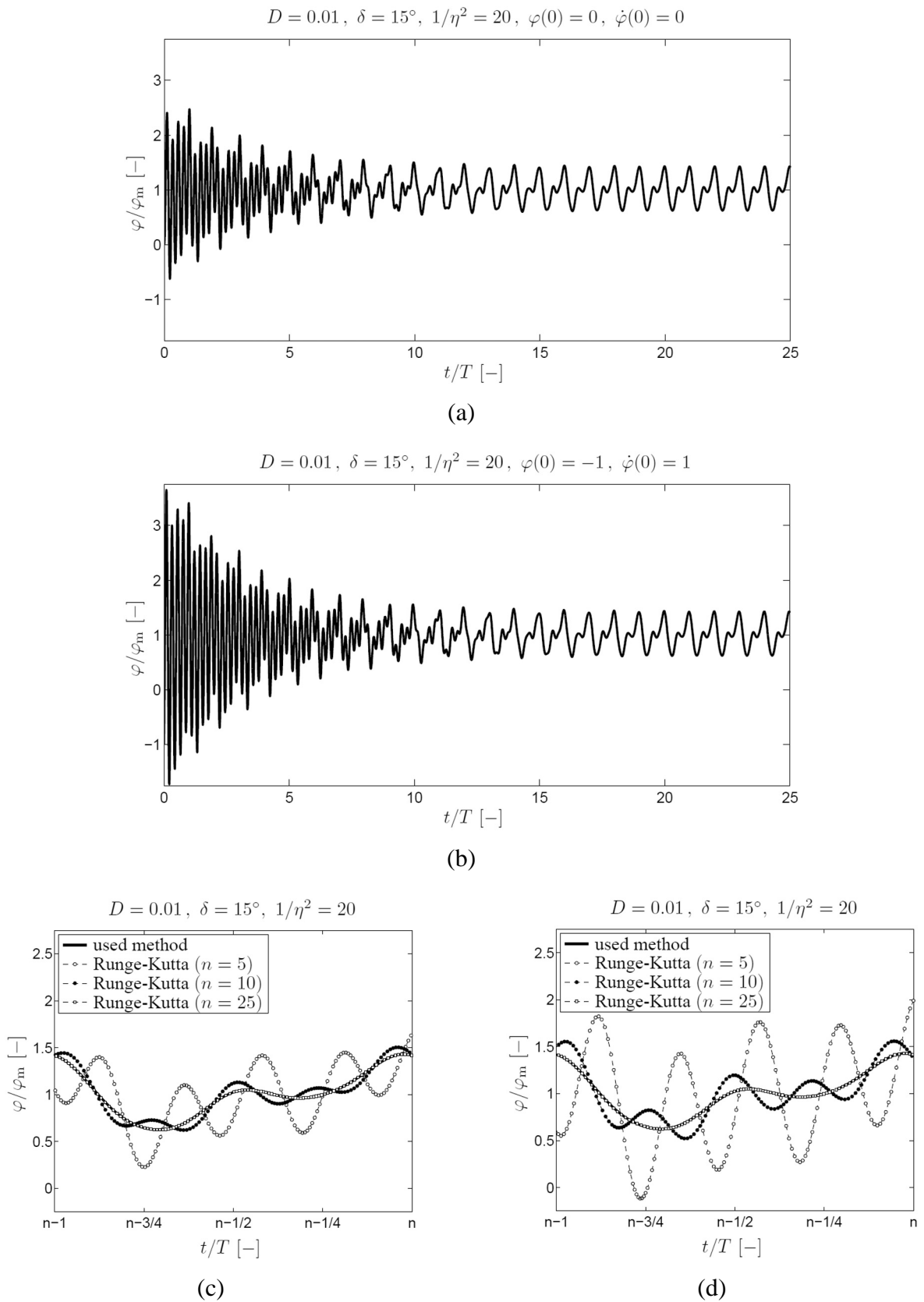
(c)

$D = 0.01$, $\delta = 15°$, $1/\eta^2 = 20$

(d)

Fig. 8. Response calculated by the used method (c), (d), and the R-KI method (a)–(d) in a stable region: the R-KI method with homogeneous (a), (c), and inhomogeneous (b), (d) initial conditions; considered periodic term "$-\varepsilon\varphi\cos 2\eta\tau$"

5. Conclusion

The presented paper brings the analytic solution of the Cardan's shaft with a small misalignment angle. With regard to this assumption, the torsional motion equation of Mathieu's type has been found. If this system is stable and is excited by a periodic function, the analytic solution is given in the form of a particular solution of investigated differential equation. The results obtained by the Runge-Kutta integration method are identical with the analytic solution in spite of different initial conditions. Then the presented method is much more efficient for finding of the steady state solution. It has been shown in a number of numerical experiments.

Moreover, the analytic solution enables to find the boundaries of (in)stability. The real eigenvalues of the matrix $(\mathbf{L}^*\mathbf{H}^*)^{-1}$ determine these borders. Furthermore, it was numerically demonstrated that the determinant of the matrix $(\mathbf{I} - \varepsilon\mathbf{L}^*\mathbf{H}^*)$ is positive only if the system is stable. The Floquet theory results were used for verification. Based on the calculations, it can be stated that the damped system with the damping ratio $D \geq 0.01$ and with the misalignment angle $\delta \leq 15°$ is always stable.

Acknowledgements

References

[1] Asokanthan, S. F., Hwang, M. C., Torsional instabilities in a system incorporating a Hooke's joint, Journal of Vibration and Acoustics 118 (3) (1996) 368–374.

[2] Asokanthan, S. F., Methan, P. A., Non-linear vibration of torsional system driven by a Hooke's joint, Journal of Sound and Vibration 233 (2) (2000) 297–310.

[3] Asokanthan, S. F., Wang, X. H., Characterization of torsional instabilities in a Hooke's joint driven system via maximal Lyapunov exponents, Journal of Sound and Vibration 194 (1) (1996) 83–91.

[4] Bulut, G., Parlar, Z., Dynamic stability of a shaft system connected through a Hooke's point, Mechanism and Machine Theory 46 (2011) 1 689–1 695.

[5] Chang, S. I., Torsional instabilities and non-linear oscillation of a system incorporating a Hooke's joint, Journal of Sound and Vibration 229 (4) (2000) 993–1 002.

[6] Duditza, F., Cardan transmissions, Editions Eyrolles, Paris, 1971. (in French)

[7] Dupal, J., Zajíček, M., Analytical solution of the drive vibration with time varying parameters, Proceedings of the ASME 2011 International Design Engineering Technical Conferences & Computers and Information in Engineering Conference, Washington DC, USA, 2011, pp. 1 365–1 370.

[8] Dupal, J., Zajíček, M., Analytical periodic solution and stability assessment of 1 DOF parametric systems with time varying stiffness, Applied Mathematics and Computation 243 (2014) 138–151.

[9] Floquet, G., Sur les équations différentielles linéaires à coefficients périodiques, Annales scientifiques de l'École Normale Supérieure 12 (1883) 47–88. (in French)

[10] Jordan, D. W., Smith, P., Nonlinear ordinary differential equations: An introduction for scientists and engineers, Oxford University Press, Oxford, 2007.

[11] Kotera, T., Instability of torsional vibrations of a system with a cardan joint, Memoirs of the Faculty of Engineering, 26, Kobe University, 1980, pp. 19–30.

[12] Murdock, J. A., Perturbations theory and methods, New York, Wiley, 1991.

[13] Porter, B., A theoretical analysis of the torsional oscillation of a system incorporating a Hooke's joint, The Journal of Mechanical Engineering Science 3 (4) (1961) 324–329.

[14] Porter, B., Gregory, R. W., Non-linear torsional oscillation of a system incorporating a Hooke's joint, The Journal of Mechanical Engineering Science 5 (2) (1963) 191–200.

[15] Porter, B., Non-linear torsional oscillation of a two-degree-of-freedom system incorporating a Hooke's point, Proceedings of the Royal Society of London Series A 277, 1964, pp. 92–106.

[16] Watson, I., Prusty, B. G., Olsen, J., Conceptual design optimisation of a constant-velocity coupling, Mechanism and Machine Theory 68 (2013) 18–34.

[17] Zahradka, J., Torsional vibrations of a non-linear driving system with cardan shafts, Journal of Sound and Vibration 26 (4) (1973) 533–550.

[18] Zeman, V., Stability of motion of mechanical systems with joints, Acta Technica CSAV 1 (1977) 52–62.

[19] Zeman, V., Dynamik der Drehsysteme mit Kardangelenken, Mechanism and Machine Theory 13 (2) (1978) 107–118. (in German)